

A symmetry-breaking inertial bifurcation in a cross-slot flow



R.J. Poole^a, G.N. Rocha^b, P.J. Oliveira^{b,*}

^a School of Eng., University of Liverpool, Liverpool L69 3GH, UK

^b Departamento de Engenharia Electromecânica, Universidade da Beira Interior, CEFT Research Unit (FEUP, Porto), Covilhã 6201-001, Portugal

ARTICLE INFO

Article history:

Received 13 July 2013

Received in revised form 9 October 2013

Accepted 8 January 2014

Available online 24 January 2014

Keywords:

Cross-slot geometry

Bifurcation

Laminar flow

Asymmetry

ABSTRACT

In the current paper we investigate, using a numerical technique, a new bifurcation phenomenon for a Newtonian fluid flowing through a two-dimensional so-called “cross-slot” geometry. A cross-slot, or cross-channel, geometry is formed by an “horizontal” planar channel along which two incoming fluid streams are made to impinge on each other, and an intersecting “vertical” channel which carries the outlet flow, with the other two streams now moving away from the central section and leaving through the vertical channel exits. At low Reynolds numbers (Re) the flow remains steady and symmetric and identical regions of standing recirculation attached to the four corners increase linearly in size with Re . At a critical Reynolds number ($=1490 \pm 10$) a supercritical pitchfork bifurcation is observed beyond which the unstable symmetrical solution is replaced by a pair of steady asymmetric solutions (each corresponding to larger recirculation regions on one vertical sidewall). The dynamics of the bifurcation are investigated in detail and a comparison made with the bifurcation observed for inertialess viscoelastic fluid flow.

© 2014 Elsevier Ltd. All rights reserved.

1. Introduction

Bifurcations in fluid flows occur frequently [9]. Typically, beyond some critical value of the Reynolds number the solution branch of the “simple” base state, e.g. steady and/or symmetric, becomes unstable and is replaced with a more complex state or states. In the current paper we are interested in a particular class of bifurcation for internal duct flows where symmetry-breaking bifurcations occur but the bifurcated flow remains steady. In particular we are concerned with a “cross-slot”, or “cross-channel”, geometry formed by an “horizontal” planar channel along which two incoming fluid streams are made to impinge on each other, and an intersecting “vertical” channel which carries the outlet flow, with the other two streams now moving away from the central section and leaving through the vertical channel exits.

Perhaps the most famous, and certainly most studied, symmetry-breaking bifurcation occurring in internal duct flows is the case of flow through planar sudden expansions. For Newtonian fluids, as was first documented in Abbott and Kline [1], above a critical Reynolds number the flow field downstream of the expansion exhibits a stable asymmetric flow state (or, more precisely, two stable anti-symmetric flow states each corresponding to a shorter recirculation region attached to one of the two downstream walls). The critical Reynolds number at which the flow becomes asymmetric is dependent

on the expansion ratio of the expansion (i.e. the ratio of the downstream to upstream channel heights) and, for three dimensional flows, the aspect ratio (i.e. the ratio of channel width to inlet channel or step height). Indeed the asymmetry is completely absent for expansion ratios less than 1.5. This asymmetry has been observed in both experimental ([7,12] for example) and numerical [6,11,19,21,26] investigations. Drikakis [11] conducted an extensive study on the effect of expansion ratio and was able to demonstrate that the critical Reynolds number for asymmetric flow to occur decreases with increasing expansion ratio. For example for a 1:2 expansion the critical Re , based on the upstream channel maximum velocity and upstream channel height, is 216 which reduces to 52 for a 1:4 expansion and then to 28 for a 1:8 expansion. These critical Reynolds numbers are affected by the non-Newtonian character of the fluids, as shown by Neofytou and Drikakis [19] for Generalised Newtonian Fluids (viscous, shear-thinning), and Oliveira [21] and Rocha et al. [26] for viscoelastic fluids (constant-viscosity with elasticity). More recently evidence has emerged that even axisymmetric sudden expansions can also display stable asymmetric states [18], although in this case it appears a finite-amplitude perturbation is required to “kick” the solution onto the asymmetric branch in comparison to the linear instability observed in the planar case [29]. Planar sudden contractions have been significantly less studied than their sudden expansion counterparts. Chiang and Sheu [8] showed using a numerical technique that a supercritical pitchfork bifurcation occurs even for planar contraction flows if the Reynolds number is driven to high enough values. This bifurcation is related

* Corresponding author. Fax: +351 275 329 972.

E-mail address: pjpo@ubi.pt (P.J. Oliveira).

to the formation of lip vortices of differing size at the entrance to the smaller channel. Although for small contraction ratios the Reynolds numbers required appear unreasonably high for laminar flow conditions to be maintained, for example at a contraction ratio (CR) of two the critical Reynolds number for bifurcation is approximately 3080, at higher contraction ratios the Reynolds numbers at which asymmetric flow appears are more modest; for $CR = 8$, $Re_{cr} = 1100$ for example.

The emerging field of microfluidics has led to the discovery of a novel bifurcation in an inherently three-dimensional flow. One of the most basic microfluidic mixing geometries, which can be easily fabricated and integrated into more complex mixing geometries, first presented by Kockmann et al. [17], is a planar T-channel with two square inlets and an outlet of equal combined area (i.e. maintaining a constant bulk velocity in each channel arm). In this geometry, two-opposing planar channel streams join and turn through 90° . In their numerical study Kockmann et al. [17] found that the resulting flow in the outlet channel can be characterised by three flow regimes during steady flow: so-called “stratified” flow, “vortex” flow and “engulfment” flow. At low flowrates, so-called stratified flow was observed and this flow regime was defined as being where the flow streamlines remain primarily unidirectional and essentially follow the curvature of the geometry. At higher flowrates, where inertial effects become important and Dean-like rolls appear in the outlet channel [10], the flow was called “vortex” flow. Finally, at a critical Reynolds number ~ 140 the flow breaks symmetry, although it remains steady, and this regime was dubbed “engulfment flow”. Since the original paper of Kockmann et al. [17], other studies have shown this effect experimentally [14,16,31] and probed the effect of different channel aspect ratios on the critical Reynolds number [25,30]. Recently, Fani et al. [15] have conducted linear stability analysis of the engulfment regime in this T-mixer geometry with 3 arms, which is the closest in terms of geometrical configuration to the 4-arms cross-slot arrangement considered in the present work. For the cross-slot flow, no linear stability analysis could be found in the literature which is not surprising since the bifurcation instability we report here has not, as far as we are aware, been reported previously.

Although a detailed literature search shows that an inertial bifurcation has not previously been studied in a cross-slot geometry, such instabilities have been observed in a related class of stagnation-point flows formed by two counterflowing jets. For example, Rolon et al. [28] observed multiple steady states in experiments of opposed or counterflowing jets of air. For the case when the jet mass flow rates are equal, the stagnation point is expected to be located half-way between the two inlets. Rolon et al. [28] illustrated the existence of two stable steady states, each having a stagnation point on the axis of symmetry, but equally displaced from the centre towards one or the other jet inlet. The effect was termed “bi-stability” and the two stable flow regimes observed were mirror images of each other indicating the possible existence of a pitchfork bifurcation. Motivated by these experimental results, Pawlowski et al. [23] used a numerical technique to investigate such counterflowing jets both for planar and axisymmetric jets. The stagnation-point flows formed in the planar case exhibit both steady-state multiplicity and time-dependent behaviour, depending on the jet separation, while axisymmetric jets exhibited only a steady-state multiplicity. Their stability analysis revealed transitions between a single (symmetric) steady state and multiple steady states or periodic steady states. Of particular relevance to the cross-slot geometry is the planar case when the jet separation distance is equal to one channel width ($\alpha = 1.0$ in the nomenclature of Pawlowski et al. [23]) where a critical Reynolds number of 872 is observed. Finally, it is worth mentioning that the paper of Ait Mouheb et al. [2] show asymmetry in cross-slot experiments but at a very low Reynolds number (50). Their comparator numerical

simulations exhibit symmetry and the authors attribute the experimentally-observed asymmetry to experimental artefacts.

Aside from the basic interest in bifurcations in fluid flows as discussed above, an additional motivation for the current study was our desire to support previous work on purely-elastic instabilities in the flow of viscoelastic flow through a cross slot [4,24,27]. Motivated by the steady asymmetry observed for viscoelastic fluids in *inertialess* cross-slot flow, a natural question one might ask is whether, even for a Newtonian fluid, there will be a similar bifurcation and asymmetries at high Reynolds number, when inertial effects start dominating the dynamics of the flow. One of the purposes of the current paper is to investigate this very possibility.

The paper is structured as follows. In the following section the governing equations and the numerical method involved in their solution are discussed. This section is followed by information regarding the geometry, computational meshes and boundary conditions. A bifurcation parameter is then defined prior to the presentation of the results and accompanying discussion. Finally we draw conclusions.

2. Governing equations and numerical method

We are concerned with the isothermal, incompressible two-dimensional flow of a Newtonian fluid and hence the equations we need to solve are those of conservation of mass

$$\nabla \cdot \mathbf{u} = 0, \quad (1)$$

and momentum

$$\rho \frac{\partial \mathbf{u}}{\partial t} + \rho \nabla \cdot \mathbf{u} \mathbf{u} = -\nabla p + \nabla \cdot \boldsymbol{\tau}, \quad (2)$$

where $\mathbf{u} = (u, v)$ is the local velocity vector, ρ the fluid density (assumed constant), p the pressure and $\boldsymbol{\tau}$ the stress tensor which, for a Newtonian fluid is given by

$$\boldsymbol{\tau} = \mu(\nabla \mathbf{u} + \nabla \mathbf{u}^T), \quad (3)$$

where μ is the dynamic viscosity. The numerical method applied in this work is the finite volume method. The governing equations (Eqs. (1), (2) and (3)) are discretised in space by integration over the set of control volumes forming the computational mesh, and in time over a small time step, Δt . This process results in systems of linearised algebraic equations for the equations of mass and momentum conservation jointly with the stress equation. In these equations all variables are evaluated and stored in the central position of the control volumes (cells) and the computational mesh applied for the present simulations is orthogonal. As a consequence, special procedures are required to ensure the pressure/velocity coupling and the velocity/stress coupling (following the method of Oliveira et al. [20]). For the calculation of the convective terms in the momentum Eq. (2) we use a high-resolution scheme called CUBISTA [3], with third-order accuracy in space for smooth flow, and having simultaneously both high numerical precision and good characteristics of iterative convergence. The CUBISTA scheme is implemented explicitly, except for the part corresponding to upwind fluxes which are incorporated implicitly through the coefficients. The Newtonian constitutive and the momentum conservation equations in discretised form are solved using a modified algorithm based on the SIMPLE algorithm developed by Patankar and Spalding [22] that allows, through an iterative process of pressure correction, to guarantee the coupling of velocity and pressure, verifying the continuity equation.

3. Geometry, computational meshes and boundary conditions

The cross-slot geometry is shown schematically in Fig. 1. Flow is provided in each inlet arm with bulk velocity U and channel width

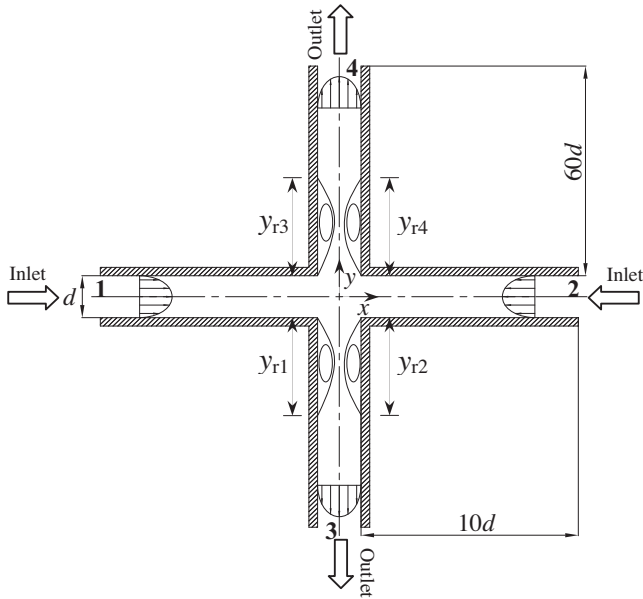


Fig. 1. Schematic of cross-slot geometry.

d , which served as velocity and length scales to define the Reynolds number $Re = \rho U d / \mu$. At the plane $x = 0$ the two streams meet and are turned through 90° into two outlet arms of identical width d . At the inlets we apply a velocity distribution corresponding to the analytical fully-developed channel-flow solution (see e.g. [32]) and at the outlets we apply a boundary condition consisting of enforcing overall mass conservation and prescribing vanishing stream-wise gradients (i.e. $\partial \phi / \partial y = 0$ where $\phi = u, v$ or $\partial p / \partial y$). At the walls we apply the no-slip condition and impenetrability (i.e. $u = v = 0$). The lengths of the inlet arms are $10d$ and the outlet arm $60d$ which we confirmed was sufficient for the flow to be fully-developed both upstream of the cross-slot and at the channel exits for all Reynolds numbers studied [13]. We confirmed that the critical Reynolds number is independent of the arm length used.

To ensure that the results obtained were mesh-independent, a solution at relatively high Reynolds number ($Re = 1400$) was obtained in two consecutively refined meshes. The computational meshes are comprised of five blocks, presented in Fig. 2, and their geometric characteristics are provided in Table 1. Each mesh has increasing mesh density closer to the cross-slot junction and a uniform cell size in the central square (Block II). The table includes the number of cells for each block, N_x along the x -direction, N_y along the y -direction and the total number of cells or control volumes (NC) inside the computational domain. The number of degrees-

Table 1

Main characteristics of the computational meshes (NC = total number of cells).

Blocks	N_x	N_y	f_x	f_y	$\Delta x_{\min} = \Delta y_{\min}$
M1					
I	50	51	0.928810	1.0	0.02
II	51	51	1.0	1.0	0.02
III	51	300	1.0	0.987882	0.02
IV	51	300	1.0	1.012267	0.02
V	50	51	1.076646	1.0	0.02
NC = 38,301 DOF = 217,806					
M2					
I	100	101	0.963748	1.0	0.01
II	101	101	1.0	1.0	0.01
III	101	600	1.0	0.993922	0.01
IV	101	600	1.0	1.0061146	0.01
V	100	101	1.037616	1.0	0.01
NC = 151,601 DOF = 909,606					

of-freedom (DOF), for each mesh, is obtained through the multiplication of NC for the six variables (two velocity components, pressure and three stress tensor components) which compose the two-dimensional geometry. The minimum cell size ($\Delta x_{\min} = \Delta y_{\min}$, these values are normalised with d) is also provided in Table 1, as are the expansion or compression factor ($f_x = \Delta x_i / \Delta x_{i-1}$ or $f_y = \Delta y_i / \Delta y_{i-1}$) for the cell size. Most of the results to be presented in this study were calculated using the base mesh (M1), and the finer (M2) mesh was obtained by doubling the number of cells along the x - and y -direction, so as to enable quantification of numerical accuracy. The tabulated data, however, were obtained with the finer mesh M2 to provide high-quality benchmark data of high accuracy. In Fig. 3 we plot the magnitude of the non-dimensional streamwise velocity along the horizontal centreline (i.e. $y = 0$) obtained in both meshes M1 and M2 at $Re = 1400$. As can be seen the agreement between the two meshes is excellent. Quantitatively, the negligible differences in the two meshes are highlighted by a difference of less than 0.7% in the length of the recirculation zones. As it is an integral quantity, a slightly larger difference in the two meshes is observed for the maximum strength of the recirculation ($\sim 3.5\%$). At higher Reynolds number, beyond bifurcation, the differences in recirculation lengths determined using M1 and M2 rise to about 4%. Since the spatial discretisation of the numerical method is second order (shown in a number of previous works, e.g. [3,21]), the numerical error reduces by a factor of four when mesh spacing is halved (i.e. as is done between mesh M1 and M2), therefore we estimate the results of mesh M2 to be accurate to better than 1%.

Additional evidence regarding convergence with mesh refinement is provided in Fig. 4 which shows convergence plots for the vortex sizes (Y_r) and intensities (ψ_r) at a particular value of the

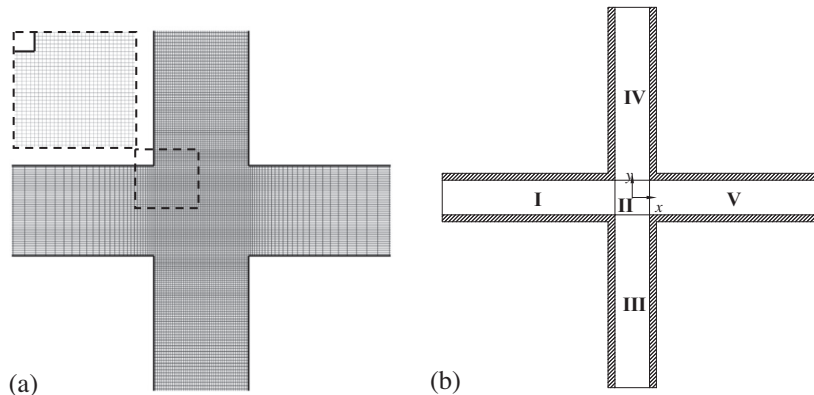


Fig. 2. (a) Mesh illustrating concentration of cells close to cross-slot ($-2 \leq x/d, y/d \leq 2$) and uniform cell distribution in central square; (b) naming convention for computational blocks.

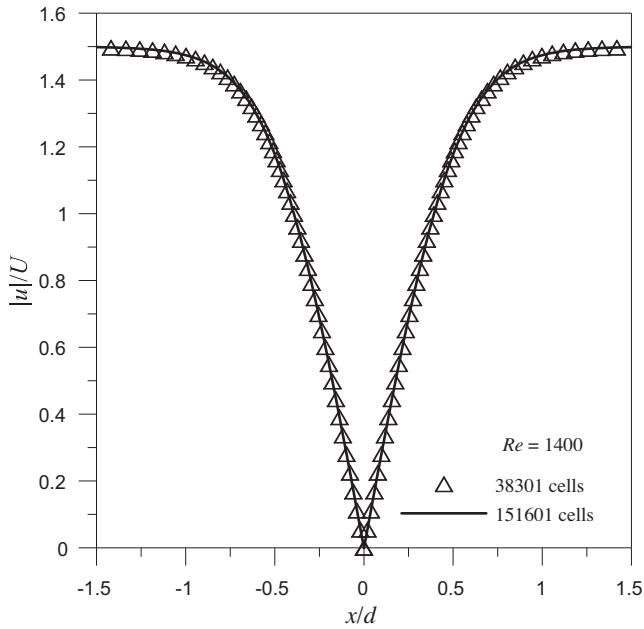
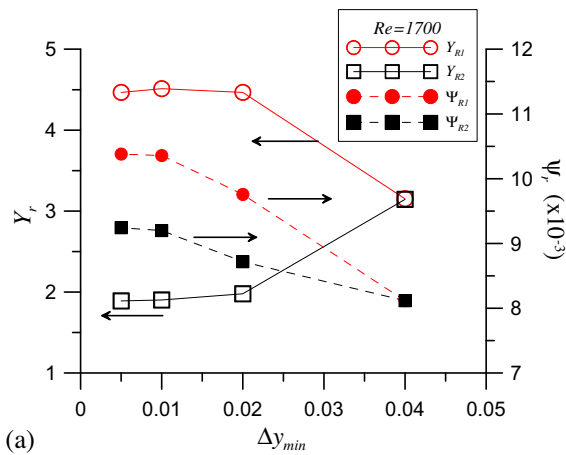
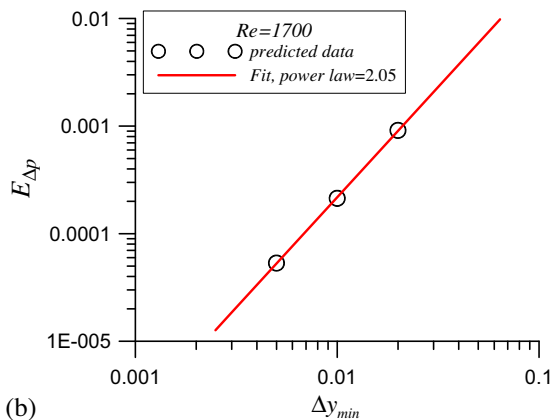


Fig. 3. Effect of mesh refinement on the magnitude of the non-dimensional streamwise velocity along horizontal centreline through the cross slot at $Re = 1400$.



(a)



(b)

Fig. 4. Convergence with mesh refinement at $Re = 1700$: (a) vortex lengths (open symbols, left y-axis) and vortex intensities (closed symbols, right y-axis) as a function of minimum mesh spacing; (b) convergence rate of overall pressure drop (Δp) in log–log scale (symbols – data; line – power law fit).

Reynolds number. Here we chose $Re = 1700$ for which the flow has already bifurcated (see Figs. 8 and 9), having a small and a larger eddy on either side of the vertical walls, and therefore offering a more stringent test than the situation at lower Re , prior to bifurcation. In this figure the finest mesh (M3) has 4 times more cells than M2 of Table 1, namely $NC = 603,201$, $DOF = 3,619,206$, with a minimum mesh spacing of $\Delta y_{\min} = \Delta x_{\min} \cong 1/200 = 0.005$. There is clearly a strong indication of convergence in Fig. 4(a), but it should be remarked that since both Y_r and ψ_r are not yet in the so-called asymptotic convergence range ($\phi = \phi_0 + C\Delta y^p$, ϕ being any solution functional), the estimated rates of convergence are either below or above the expected $p = 2$. The overall pressure drop (Δp), between inlet and one of the outlets, shows however second-order convergence rate as illustrated in Fig. 4(b) where we plot the error of Δp calculated as $E_{\Delta p} = |\Delta p - \Delta p_{\text{extrap}}|$, with the extrapolated value from $\Delta p_{\text{extrap}} = (4\Delta p_3 - \Delta p_2)/3$; the rate of decay is: $p = \log((\Delta p_1 - \Delta p_2)/(\Delta p_2 - \Delta p_3))/\log 2 = 2.01$ (Δp_i are the Δp predicted on the 3 meshes M1, M2 and M3 for $i = 1, 2, 3$).

4. Bifurcation parameter

To estimate the critical Reynolds number for the bifurcation to asymmetric flow we define an asymmetry parameter

$$DY = -\frac{Y_{r2} - Y_{r1}}{\frac{1}{2}(Y_{r2} + Y_{r1})} = \frac{Y_{r4} - Y_{r3}}{\frac{1}{2}(Y_{r4} + Y_{r3})}, \quad (4)$$

where, as highlighted in Fig. 1, Y_{r1} is the length (normalised with d) of the recirculation region attached to the west face of the south outlet channel, Y_{r2} is the length of the recirculation region attached to the east face of the south outlet channel, Y_{r3} is the length of the recirculation region attached to the west face of the north outlet channel and Y_{r4} is the length of the recirculation region attached to the east face of the north outlet channel. For a symmetric flow $|Y_{r1}| = |Y_{r2}| = |Y_{r3}| = |Y_{r4}|$ and $DY = 0$ whereas, beyond the bifurcation, we observe that $|Y_{r1}| = |Y_{r3}|$, $|Y_{r2}| = |Y_{r4}|$ and $DY \neq 0$. An alternative bifurcation parameter is provided by the lateral displacement of the stagnation point, $DX = (x_c - 0)/d$. Our results indicate that the point of zero velocity $u = v = 0$ always remains in the horizontal symmetry line of the cross-slot (i.e. $y = 0$), remaining at the centre of the cross-slot ($x = y = 0$) while the flow is at Reynolds numbers below the critical conditions, and becomes displaced to one side or the other once the flow becomes supercritical.

5. Results and discussion

5.1. Symmetric flow prior to bifurcation

With increasing flowrate, four identical standing recirculating bubbles attached at the four corners of the cross-slot geometry grow significantly. In Fig. 5 the effect of increasing inertia on the size of these recirculation regions is highlighted for $200 \leq Re \leq 1000$. Only one quarter of the cross-slot geometry is shown due to the symmetric nature of the flow field under these conditions. In this regime the length of the recirculation regions is found to increase linearly with Reynolds number ($\sim 0.002Re$) much as observed in planar sudden expansions for example [11]. Table 2 quantifies the growth in the length of the reattachment regions and confirms that, at least for $Re < 1500$, the four standing recirculation regions are equal in size. (NB: These data were based on simulations with the finer mesh M2.) The intensity of the recirculation regions ψ_r , calculated by the amount of recirculating flow normalised by the inlet flow rate and shown in Fig. 6, also grows monotonically with Reynolds number in this region but the relationship is not linear. Fig. 7 shows that the transverse distance of the eye of the recirculation to the nearest wall grows rapidly for

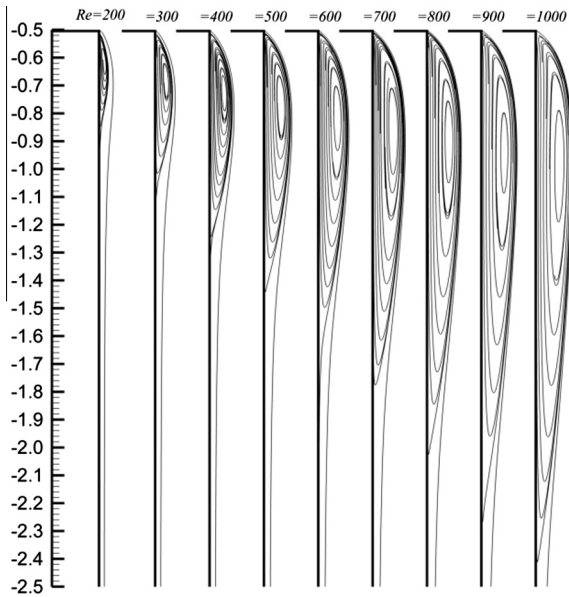


Fig. 5. Effect of inertia on size of recirculation region in symmetric regime ($Re \leq 1000$). NB: Only one quarter of the geometry is shown due to fourfold symmetry.

Table 2

Variation of recirculation zone length on each wall with Reynolds number (data based on M2).

Re	Y_{r1}	Y_{r2}	Y_{r3}	Y_{r4}
200	-0.331	-0.331	+0.331	+0.331
400	-0.744	-0.744	+0.744	+0.744
600	-1.137	-1.137	+1.137	+1.137
800	-1.534	-1.534	+1.534	+1.534
1000	-1.937	-1.937	+1.937	+1.937
1200	-2.343	-2.343	+2.343	+2.343
1400	-2.751	-2.751	+2.751	+2.751
1480	-2.914	-2.916	+2.914	+2.916
1500	-2.525	-3.347	+2.525	+3.347
1520	-2.325	-3.585	+2.325	+3.585
1540	-2.209	-3.750	+2.209	+3.750
1560	-2.130	-3.884	+2.130	+3.884
1580	-2.072	-3.998	+2.072	+3.998
1600	-2.027	-4.101	+2.027	+4.101
1700	-1.901	-4.512	+1.901	+4.512
1800	-1.846	-4.837	+1.846	+4.837
1900	-1.820	-5.115	+1.820	+5.115
2000	-1.809	-5.360	+1.809	+5.360

Re up to ≈ 800 and then it remains approximately constant at a value of $0.095d$ because interaction with the bubble on the opposite wall restrains its spatial extent for further growth. In contrast the distance of the recirculation centre to the corner grows linearly with Re (Y_r data discussed below and shown in Fig. 9). Since the amount of recirculating flow is proportional to the area of the bubble, the reduction of the rate of growth of ψ_r seen in Fig. 6 at $Re \approx 800$ is due to spatial limitations in the transversal direction.

5.2. Bifurcated asymmetric flow

Beyond $Re = 1500$, as shown by the streamline images in Fig. 8, the flow loses stability and breaks symmetry about the vertical centreline plane ($x = 0$). The symmetry-breaking bifurcation is reflected in the asymmetrical growth of the two recirculation regions and is especially noticeable at $Re = 1600$ (and beyond, not shown). Although symmetry is broken about the vertical centreline, symmetry is retained about the horizontal centreline (i.e. $y = 0$). As a

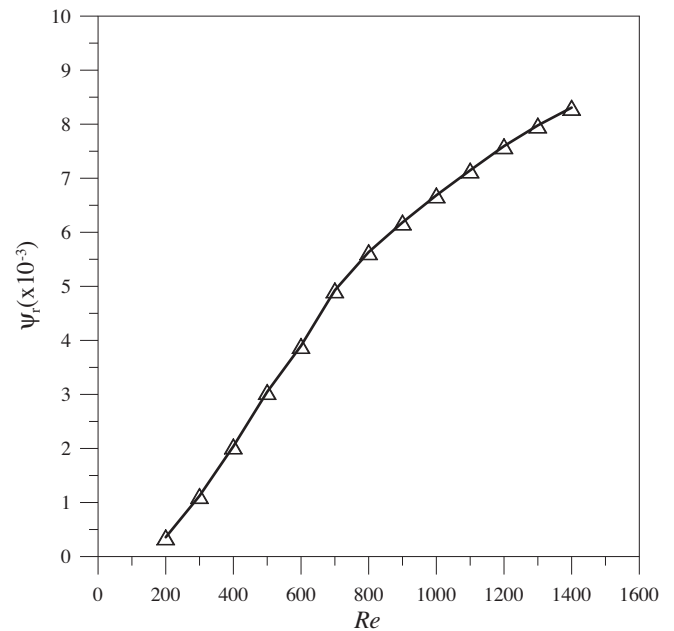


Fig. 6. Effect of inertia on intensity of recirculation region in symmetric regime ($Re \leq 1500$).

consequence of this partial symmetry only half the geometry is shown in Fig. 8 to better highlight the asymmetry. In addition, as shown in Table 2, the partial symmetry is reflected in the fact that $Y_{r1} = -Y_{r3}$ and $Y_{r2} = -Y_{r4}$. Thus the nature of the symmetry-breaking bifurcation in this inertial Newtonian case is significantly different to the purely-elastic asymmetry observed in the viscoelastic cross-slot flow where the bifurcated flow retains partial symmetry about the cross-slot diagonal planes (i.e. $y = \pm x$) [24].

The bifurcation is further illustrated in Fig. 9 where the variation of the length of the recirculation region with Reynolds number is shown. Due to the (partial) symmetrical nature of the results data is only shown for Y_{r3} and Y_{r4} . The pitchfork nature of the bifurcation is clearly apparent. Also shown in Fig. 9 is the length of recirculation for a quarter cross-slot geometry in which symmetry is imposed on the flow through the boundary conditions. Very small graduations in Re close to the bifurcation point allowed us to identify the critical Reynolds number as $Re_{cr} = 1490 \pm 10$. Below Re_{cr} , as expected, the recirculation regions in the full and symmetry-imposed geometries are identical. Beyond Re_{cr} , the symmetric solution branch is unstable in the full cross-slot and two stable asymmetric branches appear (corresponding to the shorter recirculation region attached to either the west or east side downstream walls). By contrast in the symmetry-imposed geometry the recirculation regions grow linearly (and symmetrically) with increasing inertia for all Reynolds numbers studied.

The variation of the bifurcation parameter DY (Eq. (4)) with Reynolds number is shown in Fig. 10. Below Re_{cr} , $DY = 0$. Close to Re_{cr} , DY varies like $\sim \sqrt{Re - Re_{cr}}$ typical of supercritical pitchfork bifurcations. Fitting the relevant data close to critical conditions indicates $DY = A\sqrt{Re - Re_{cr}}$ with $A = 0.06$, shown by the solid line in Fig. 10. Beyond Re_{cr} the symmetric solution branch – shown in Fig. 10 by dotted lines – becomes unstable and is replaced by two asymmetric branches (corresponding to $\pm DY$). Since the two larger vortices stay attached to the same side of the vertical walls, the “central” stagnation point must be shifted to the opposite side, which may lie on either the negative or positive portions of the x -axis, depending on conditions that are not controllable *a priori* (our numerical technique was able to capture both branches

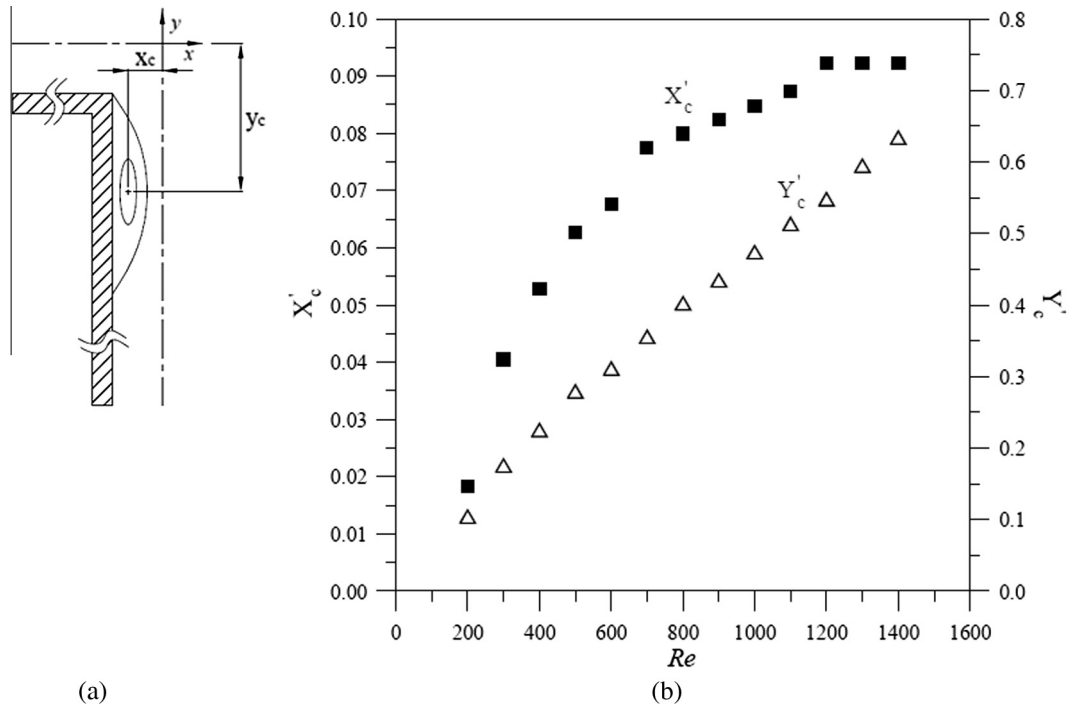


Fig. 7. (a) Definition of lateral ($X'_c = (\frac{1}{2}d - |x_c|)/d$) and streamwise ($Y'_c = (|y_c| - \frac{1}{2}d)/d$) distances to centre of recirculation eye in symmetric region; (b) Quantitative values of these distances and their variation with Reynolds number.

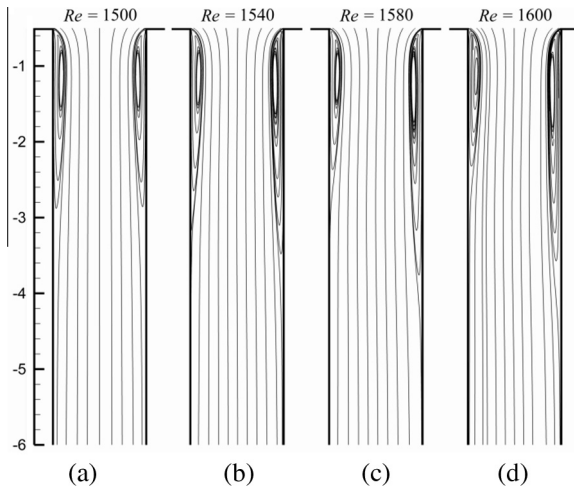


Fig. 8. Size of recirculation zones close to critical conditions (a) $Re = 1500$; asymmetric growth of recirculation regions beyond bifurcation: (b) $Re = 1540$; (c) $Re = 1580$ and (d) $Re = 1600$.

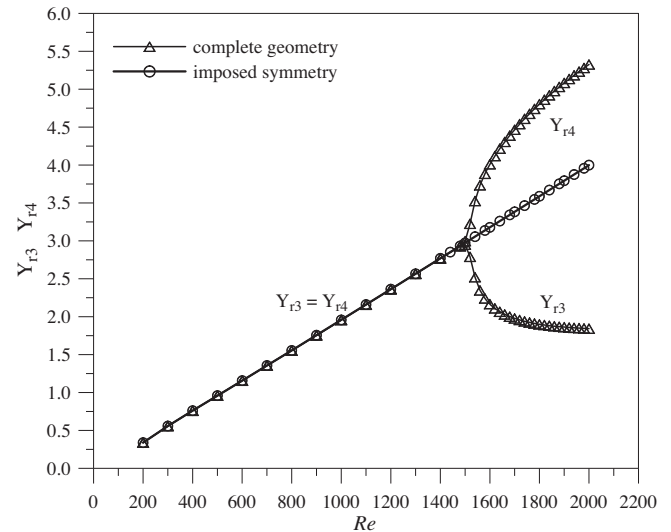


Fig. 9. Influence of inertia (Re) upon the size of the two eddies on the upper outlet channel.

depending on initial conditions). This situation is shown in Fig. 11 which also exhibits a perfect pitchfork variation for the alternative bifurcation parameter $DX = x_c/d$ in a very similar fashion to that of DY shown in Fig. 10. For $Re < Re_{cr}$, the stagnation point remains at the geometrical centre of the cross geometry; for conditions beyond the critical condition, $Re > Re_{cr}$, it is shifted to one or the other side, albeit the relative displacement being relatively small (on the order of 1% of the channel width). It may be argued that it is this imperceptible displacement of the stagnation point which eventually triggers the asymmetric stationary state. Analogous to the well-known Coanda effect in planar expansions, initial perturbations brought about by the impinging action of the two incoming streams, may result in a lateral displacement of the stagnation point which, in turn, leads to a concomitant smaller recirculation

eddy on that side. Near the reattachment point of that recirculation region (the “eddy”) velocities are smaller and thus pressures are higher, compared to the opposite eddy on the other wall, initiating a mechanism that tends to further accentuate the differences between the two eddy sizes. For sufficiently high levels of inertia this mechanism eventually leads to two opposed eddies of differing sizes, which do not vary with time.

In order to understand the dissipative nature of the bifurcation in Fig. 12 we plot the pressure drop between the inlet to the west inlet arm and the outlet of the north outlet arm. Due to the relatively high Reynolds numbers considered here we choose to normalise this pressure drop using an inertial scaling (ρU^2 i.e. twice the so-called dynamic pressure). Also included in Fig. 12 is the

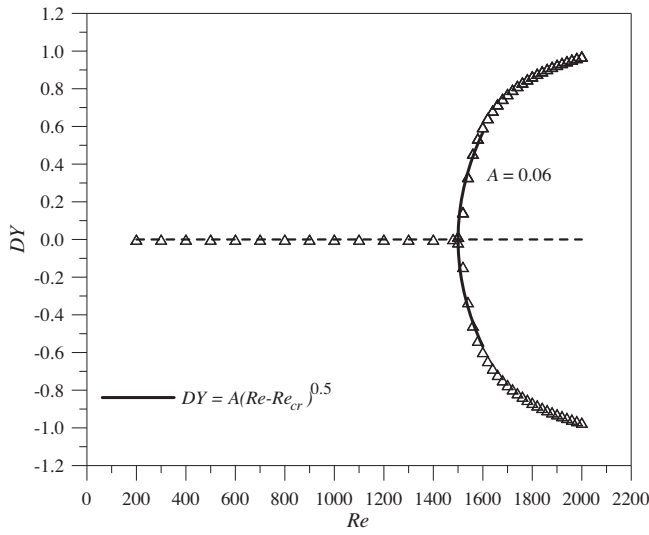


Fig. 10. Variation of bifurcation parameter with Reynolds number illustrating appearance of supercritical pitchfork bifurcation beyond $Re = 1490$.

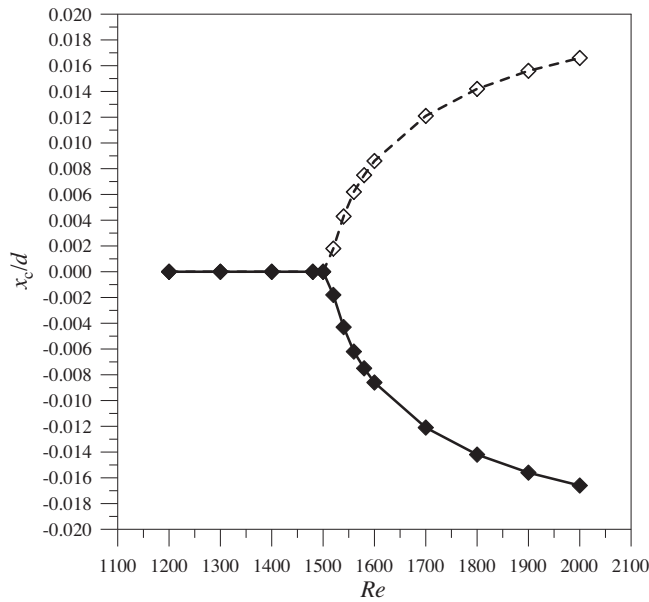


Fig. 11. Bifurcation diagram for the stagnation point lateral displacement ($DX = x_c/d$).

equivalent data for the symmetry-imposed case (1/4 cross-slot). The marginal change in the dissipation is clear in Fig. 12(a) where the two cases appear to essentially superimpose for all Reynolds numbers: only in a zoomed section, shown in Fig. 12(b), is it apparent that the bifurcated state actually leads to a slightly higher pressure drop than the symmetric case and is therefore more dissipative. Since most of the pressure drop in Fig. 12 is due to wall friction along the channels under fully-developed flow conditions (Δp_{FD} ; e.g. for $Re = 1000$, the numerically determined pressure drop is $\Delta p/\rho U^2 = 0.876$ and $\Delta p_{FD}/\rho U^2 = fL/d = 0.012 \times 70 = 0.84$, for a Fanning friction factor $f = 12/Re = 12/1000$), thus masking the amount of localised energy loss between the artificially symmetric and the naturally asymmetric flows, we have also calculated a loss coefficient defined as $K = (\Delta p - \Delta p_{FD})/\rho U^2$ and, in Fig. 13, plot this parameter as a function of Reynolds number. Here the incremental pressure loss brought about by the bifurcation becomes more evi-

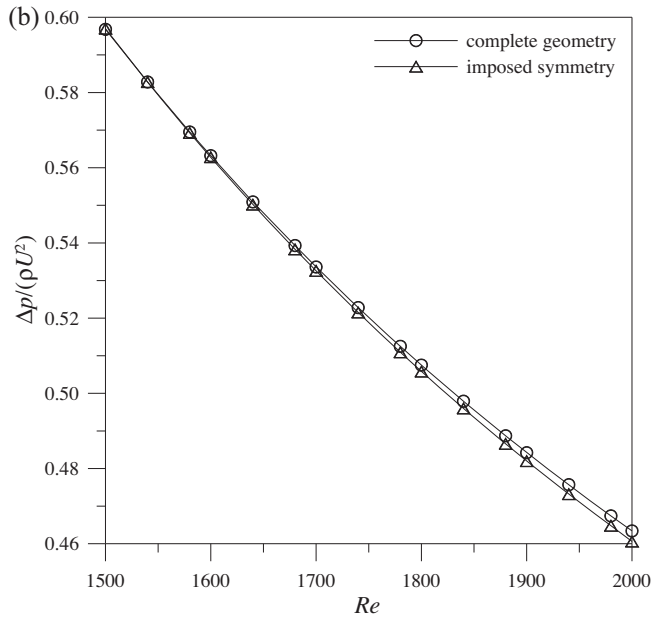
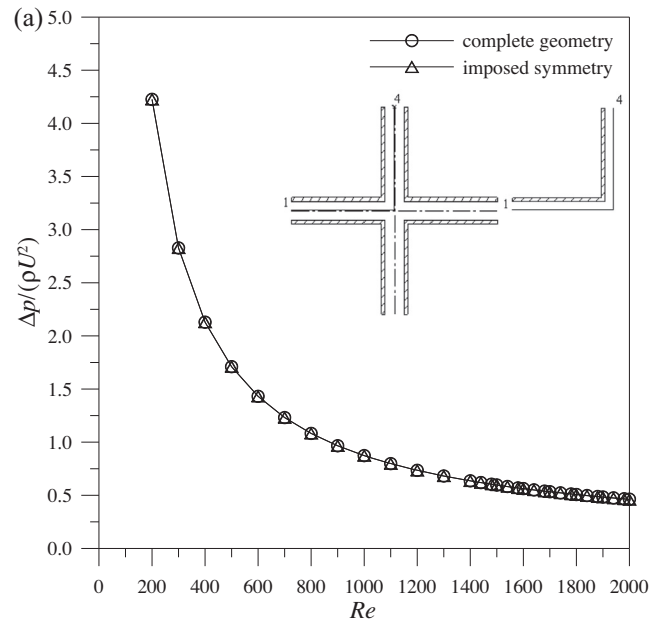


Fig. 12. Pressure-drop through the cross-slot and for a quarter (symmetry-imposed) geometry for (a) all Reynolds numbers; (b) zoomed view highlighting effect of bifurcated flow regime.

dent, as is clearly seen by a sudden increase in the derivative of the K vs. Re variation when the asymmetry sets in as compared to the trend if the flow remains symmetric. This result contrasts sharply with the asymmetry observed in inertialess viscoelastic cross-slot flow [24] where the bifurcated state leads to a sharp reduction in pressure drop.

The overall loss indicators, shown in Figs. 12 and 13, highlight the increased energy input required when the flow bifurcates to an asymmetric state, are essentially obtained from an overall energy balance where the only energy fluxes that are different at the outlet sections are the pressure terms (the kinetic energy is the same since the flow is fully developed at the exit). As a consequence these quantities do not reflect directly the changes in flow details inside the cross-slot domain. In order to better highlight differences between symmetric and asymmetric flow configurations resulting from local field variations, we choose to define a

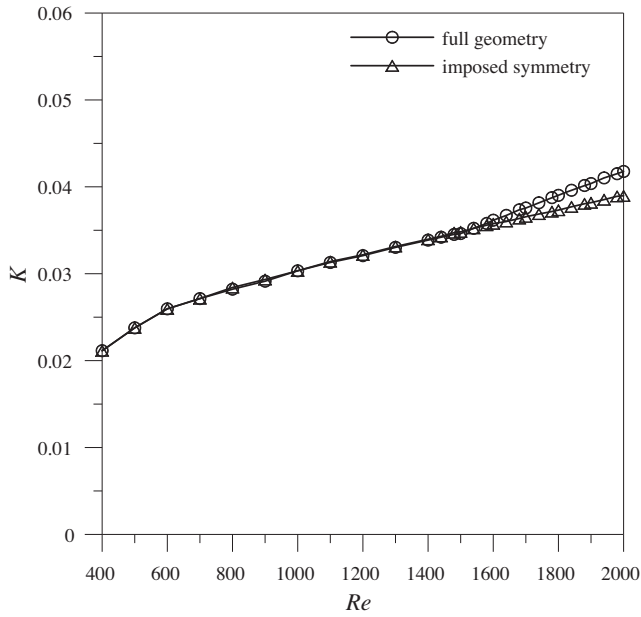


Fig. 13. Local loss coefficient as a function of Reynolds number for the full and the symmetry-imposed geometries.

kinetic-energy difference (ΔE_k) which is calculated as the sum over the entire flow domain of the local E_k minus the corresponding fully developed value, thus

$$\Delta E_k = \frac{1}{\rho U^2} \sum_{i=1}^{NC} \frac{1}{2} \rho (\mathbf{u}_i - \mathbf{u}_{i,FD})^2 \quad (5)$$

In this expression, $\mathbf{u}_i = (u_i, v_i)$ and $\mathbf{u}_i^2 = u_i^2 + v_i^2$, where index i denotes the cell in the computational mesh; for the fully-developed velocity, in terms of vector components, we have $\mathbf{u}_{i,FD} = (\pm 1.5U(1 - (y_i/\frac{1}{2}d)^2), 0)$ in the east and west inlet branches and $\mathbf{u}_{i,FD} = (0, \pm 1.5U(1 - (x_i/\frac{1}{2}d)^2))$ in the north and south outlet branches. This parameter is shown in Fig. 14 as a function of Re and a clear separation between the symmetric and bifurcated flow can be observed. The rate of increase of ΔE_k exhibits an abrupt change when $Re > 1500$ (i.e. beyond bifurcation). The data exhibits

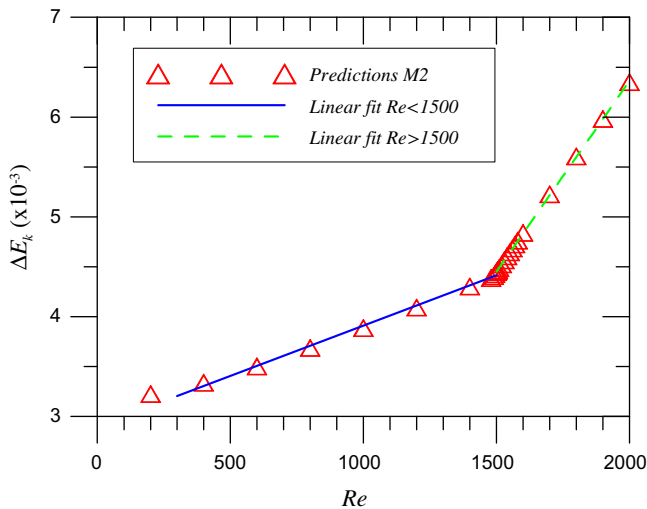


Fig. 14. Normalised excess kinetic energy as a function of Reynolds number indicating transition to asymmetric flow at $Re \approx 1500$.

a linear growth of the excess kinetic energy as $\approx 1.0(Re/1000)$ for $Re < Re_{cr}$, and as $\approx 3.8(Re/1000)$ for $Re > Re_{cr}$. There is thus a 2.8 relative increase in the growth rate of excess kinetic energy resulting from flow bifurcation.

6. Conclusions

Motivated by the steady asymmetry observed for viscoelastic fluids in *inertialless* cross-slot flow, the purpose of the current study was to investigate the possibility of a similar instability occurring in Newtonian fluids but driven by inertia. Indeed a transition is observed at a critical Reynolds number of $Re_{cr} = 1490 \pm 10$ (based on the average inlet velocity and the channel width), above which the flow becomes asymmetric but the asymmetry is significantly different from the *inertialless* viscoelastic case. While the viscoelastic instability exhibits symmetry about the cross-slot diagonal planes ($y = +x$ or $y = -x$), the current inertial Newtonian flow is symmetric about the horizontal plane ($y = 0$). For increasing Re , four identical standing recirculating bubbles are initially formed starting at the four corners of the geometry; when $Re > Re_{cr}$, the two bubbles on one side (say, $x > 0$) become larger than the two bubbles at the other side ($x < 0$). The flow remains steady. The asymmetry found is reminiscent of that occurring in flow through planar expansions (e.g. [1,11]) but occurs at higher Re . An additional difference compared to the viscoelastic case is that the stagnation point does not stay at the geometrical centre of the geometry; this is due to the fact that the two larger vortices stay on the same side of the vertical axis and therefore the stagnation point must displace to accommodate the change of the geometry of the vena-contracta defined by both recirculation regions. Another difference found from the results of the present simulations is that the excess pressure drop for the bifurcated flow is larger than the pressure drop for a corresponding symmetric-imposed case. In the viscoelastic counterpart at $Re = 0$ the fact that the energy loss was smaller for a bifurcated solution compared to the symmetric solution was used as a partial justification for the flow, under natural conditions, to “prefer” the former configuration [24]. By contrast, in the current study for a flow with significant inertial contribution (Re above about 1500), with a Newtonian fluid, we have the opposite scenario. However, as such “minimum energy dissipation” theorems (the so-called Helmholtz–Korteweg theorem, see e.g. [5]) apply in the limit of creeping flows only, this latter difference is perhaps not entirely unexpected for the *inertial* instability observed here for Newtonian fluids.

Future work will be needed to extend this investigation to the corresponding three-dimensional flow configuration, and to tackle the linear stability analysis of this type of flow, which, as evidenced by the recent contribution by Fani et al. [15] who analysed the related T-channel geometry (with 3 arms, instead of 4), represents a significant task with large computational costs. We have already started exploring 3D effects and a first important conclusion from these preliminary simulations is that in 3D the bifurcation cannot be sensed by comparing the lengths of the vortices on the two side walls, but needs other more sensitive bifurcation parameter. In this respect asymmetries in the lateral (along z) velocity profile in a line at $y = \pm d/2$ (section on the entry to the outlet channels) may offer a convenient alternative bifurcation parameter. We hope to report on 3D effects in a future study.

Acknowledgements

GNR and PJO would like to thank the financial support by Fundação para a Ciência e a Tecnologia (FCT), Portugal, through Grant SFRH/BD/22644/2005 and Project PTDC/EME-MFE/98558/2008.

References

- [1] Abbott DE, Kline SJ. Experimental investigation of subsonic turbulent flow over single and double backward facing steps. *J Basic Eng* 1962;84:317–25.
- [2] Ait Mouheeb N, Montillet A, Sollicec C, Havlica J, Lengentilhonne P, Comiti J, et al. Flow characterisation in T-shaped and cross-shaped micromixers. *Microfluid Nanofluid* 2011;10:1185–97.
- [3] Alves MA, Pinho FT, Oliveira PJ. A convergent and universally bounded interpolation scheme for the treatment of advection. *Int J Numer Method Fluid* 2003;41:47–75.
- [4] Arratia PE, Thomas CC, Diorio JD, Gollub JP. Elastic instabilities of polymer solutions in cross-channel flow. *Phys Rev Lett* 2006;96:144502.
- [5] Astarita G. Variational principles and entropy production in creeping flow of non-Newtonian liquids. *J Non-Newt Fluid Mech* 1977;2:343–51.
- [6] Battaglia F, Tavener SJ, Kulkarni AK, Merkle CL. Bifurcation of low Reynolds number flows in symmetric channels. *AIChE J* 1997;35:99–105.
- [7] Cherdron W, Durst F, Whitelaw JH. Asymmetric flows and instabilities in symmetric ducts with sudden expansions. *J Fluid Mech* 1978;84:13–31.
- [8] Chiang TP, Sheu TWH. Bifurcations of flow through plane symmetric channel contraction. *J Fluid Eng* 2002;124:144–51.
- [9] Crawford JD, Knobloch E. Symmetry and symmetry-breaking bifurcations in fluid-dynamics. *Annu Rev Fluid Mech* 1991;23:341–87.
- [10] Dean WR. Note on the motion of fluid in a curved pipe. *Phil Mag* 1927;20:208–23.
- [11] Drikakis D. Bifurcation phenomena in incompressible sudden expansion flows. *Phys Fluids* 1997;9:76–86.
- [12] Durst F, Pereira JCF, Tropea C. The plane symmetric sudden-expansion flow at low Reynolds numbers. *J Fluid Mech* 1993;248:567–81.
- [13] Durst F, Ray S, Ünsal B, Bayoumi OA. The development lengths of laminar pipe and channel flows. *J Fluids Eng* 2005;127(6):1154–60.
- [14] Engler M, Kockmann N, Kiefer T, Woias P. Numerical and experimental investigations on liquid mixing in static micromixers. *Chem Eng J* 2004;101(1–3):315–22.
- [15] Fani A, Camarri S, Salvetti MV. Investigation of the steady engulfment regime in a three-dimensional T-mixer. *Phys Fluids* 2013;25:064102.
- [16] Hoffmann M, Schlüter M, Rübiger N. Experimental investigation of liquid–liquid mixing in T-shaped micro-mixers using -LIF and -PIV. *Chem Eng Sci* 2006;61(9):2968–76.
- [17] Kockmann N, Föll C, Woias P. Flow regimes and mass transfer characteristics in static micro-mixers. In: *The international society for optical engineering*. San Jose, CA: SPIE; 2003.
- [18] Mullin T, Seddon JRT, Mantle MD, Sederman AJ. Bifurcation phenomena in the flow through a sudden expansion in a circular pipe. *Phys Fluids* 2009;21(1):014110.
- [19] Neofytou P, Drikakis D. Non-Newtonian flow instability in a channel with a sudden expansion. *J Non-Newt Fluid Mech* 2003;111:127–50.
- [20] Oliveira PJ, Pinho FT, Pinto GA. Numerical simulation of non-linear elastic flows with a general collocated finite-volume method. *J Non-Newton Fluid Mech* 1998;79:1–43.
- [21] Oliveira PJ. Asymmetric flows of viscoelastic fluids in symmetric planar expansion geometries. *J Non-Newton Fluid Mech* 2003;114:33–63.
- [22] Patankar SV, Spalding DB. Calculation procedure for heat, mass and momentum transfer in three-dimensional parabolic flows. *Int J Heat Mass Transfer* 1972;25:17–87.
- [23] Pawlowski RP, Salinger AG, Shadid JN, Mountziaris TJ. Bifurcation and stability analysis of laminar isothermal counterflowing jets. *J Fluid Mech* 2006;55:117–39.
- [24] Poole RJ, Alves MA, Oliveira PJ. Purely elastic flow asymmetries. *Phys Rev Lett* 2007;99:164503.
- [25] Poole RJ, Alfateh M, Gauntlett AP. Bifurcation in a T-channel junction: effects of aspect ratio and shear-thinning. *Chem Eng Sci* 2013;104:839–48.
- [26] Rocha GN, Poole RJ, Oliveira PJ. Bifurcation phenomena in viscoelastic flows through a symmetric 1:4 expansion. *J Non-Newt Fluid Mech* 2007;141:p1–p17.
- [27] Rocha GN, Poole RJ, Alves MA, Oliveira PJ. On extensibility effects in the cross-slot flow bifurcation. *J Non-Newt Fluid Mech* 2009;156:58–69.
- [28] Rolon JC, Veynante D, Martin JP. Counterjet stagnation flows. *Exp Fluids* 1991;11:313–24.
- [29] Sanmiguel-Rojas E, Mullin T. Finite-amplitude solutions in the flow through a sudden expansion in a circular pipe. *J Fluid Mech* 2012;691:201–13.
- [30] Soleymani A, Kolehmainen E, Turunen I. Numerical and experimental investigations of liquid mixing in T-type micromixers. *Chem Eng J* 2008;135S:219–28.
- [31] Thomas S, Ameel TA. An experimental investigation of moderate Reynolds number flow in a T-Channel. *Exp Fluids* 2009;49(6):1231–45.
- [32] White FM. *Viscous fluid flow*. McGraw-Hill; 1991.